2017-07-01

Formulation, characterisation and stability assessment of a food derived 1 tripeptide, Leucine-Lysine-Proline loaded chitosan nanoparticles

M.K. Danish
Technological University Dublin

Giuliana Vozza
Technological University Dublin

Hugh Byrne
Technological University Dublin, hugh.byrne@tudublin.ie

Recommended Citation

"Formulation, characterisation and stability assessment of a food derived tripeptide, Leucine-Lysine-Proline loaded chitosan nanoparticles", Minna K. Danish, Giuliana Vozza, Hugh J. Byrne, Jesus M. Frias, Sinéad M. Ryan, Journal of Food Science: Food Engineering, Materials Science, and Nanotechnology, June (2017) DOI: 10.1111/1750-3841.13824

Formulation, characterisation and stability assessment of a food derived tripeptide, Leucine-Lysine-Proline loaded chitosan nanoparticles

Minna Khalid [1 2], Giuliana Vozza[1 2], Hugh J. Byrne [2], Jesus M. Frias[1], Sinéad M. Ryan[3]

[1] School of Food Science and Environmental Health, Dublin Institute of Technology, Marlborough Street, Dublin 1, Ireland

[2] FOCAS Research Institute, Dublin Institute of Technology, Kevin Street, Dublin 8, Ireland

[3] School of Veterinary Medicine, University College Dublin, Belfield, Dublin 4, Ireland

[*] Corresponding author. E-mail: Jesus.Frias@dit.ie

Abstract

The chicken or fish derived tripeptide, Leucine-Lysine-Proline (LKP), inhibits the Angiotensin Converting Enzyme and may be used as an alternative treatment for pre-hypertension. However, it has low permeation across the small intestine. The formulation of LKP into a nanoparticle (NP) has the potential to address this issue. LKP-loaded NPs were produced using an ionotropic gelation technique, using chitosan (CL113). Following optimisation of unloaded NPs, a mixture amount design was constructed using variable concentration of CL113 and tripolyphosphate at a fixed LKP concentration. Resultant particle sizes ranged from 120-271 nm, zeta potential values from 29-37 mV and polydispersity values from 0.3-0.6. A ratio of 6:1 (CL113: TPP) produced the best encapsulation of approximately 65%. Accelerated studies of the loaded nanoparticles indicated stability under normal storage conditions (room temperature). Cytotoxicity assessment showed no significant loss of cell viability and *in vitro* release studies indicated an initial burst followed by a slower and sustained release.

Keywords: chitosan nanoparticles; food derived peptide; mixture amount design; accelerated thermal stability analysis; ACE inhibition

1. Introduction

A number of synthetic antihypertensive drugs (ACE inhibitors) are currently available on the market (e.g. captopril, lasinopril and enalapril) but all have been reported to have associated adverse side effects, such as coughing, dizziness, loss of taste and skin rashes and poor pharmacokinetics with a short half life, resulting in the requirement of frequent dosage (Bougatef et al., 2008). Therefore, natural ACE inhibitors, isolated from food sources, have attracted increasing attention in recent years, in the search to find a safer and more economical approach for the consumers (Bougatef et al., 2008). Peptides derived from food sources have been reported to have health benefits such as hypotensive activity, due to their Angiotensin Converting Enzyme (ACE) inhibitory activity (Berilyn et al., 2016; Li et al., 2016). Using DNA microarray experiments it was found that other mechanisms can also contribute to the decrease of blood pressure for bioactive tripeptides (Yamaguchi, Kawaguchi, & Yamamoto, 2009) reducing the side effects of ACE inhibition. However, exploitation of the potential nutraceutical benefits of these peptides in general is known to face a number of challenges. Insufficient gastric residence time, low permeation and/or solubility within the gut, chemical degradation within the gastrointestinal tract (GIT) due to low pH, enzymatic degradation, and the presence of other nutrients (in food), all limit the bioavailability of bioactive peptides by the oral delivery route (Braithwaite et al., 2014; Ma, 2014; Segura-Campos, Chel-Guerrero, Betancur-Ancona, & Hernandez-Escalante, 2011). A number of researchers have attempted to formulate peptides into oral delivery systems for example by the addition of absorption enhancers (Choonara et al., 2014), enzyme inhibitors (Bruno, Miller, & Lim, 2013), hydrogels (Sharpe, Daily, Horava, & Peppas, 2014), liposomes (Takahashi, Uechi, Takara, Asikin, & Wada, 2009) and nanoparticles (Yao, McClements, & Xiao, 2015).

Leucine-Lysine-Proline is a tripeptide, derived from chicken muscle, which has shown *in vitro* ACE inhibitory activity, having a mean inhibitory concentration (IC_{50}) of 0.32µM (Zhou, Du, Ji, & Feng, 2012). In addition, LKP has been shown to elicit a significant reduction of blood pressure in spontaneously hypertensive rats (SHR) when delivered intravenously, 10mg/kg^{-1} producing a reduction in systolic blood pressure of 75mmHg, compared to an oral dose of 60mg/kg^{-1}, which resulted in a reduction of 18mmHg (Fujita, Yokoyama, Yoshikawa, Iroyukifujita, & Eiichiyokoyama, 2000). Captopril, a synthetic oral ACE inhibitor drug used for the treatment of hypertension, has been reported by Quiñones *et al.* (2015) to show a maximum *in vivo* change in SHR of 60.5 ± 2.7 mmHg, 4 hours post-administration, when 50mg/kg was given orally . Recent studies have shown that LKP is stable in the GIT but with lower permeation than the market drugs, across the intestine at its target site, the small intestine (Gleeson, Heade, Ryan, & Brayden, 2015). Formulation into nanoparticles (NPs) for oral delivery can enhance the bioavailability of an encapsulated peptide drug and consequently improve its pharmacokinetics and stability (Patel, Patel, Yang, & Mitra, 2014; Ryan et al., 2013). Stable NPs with particle sizes ranging between 100-500nm (des Rieux, Fievez, Garinot, Schneider, & Préat, 2006), zeta potential values (ZP) ≥ 30mV (Lakshmi & Kumar, 2010), polydispersity (PDI) < 0.400 (Abdel-Hafez, Hathout, & Sammour, 2014a) and maximum encapsulation efficiency are ideal characteristics for oral supplementation.

Chitosan is a linear polysaccharide, prepared by N-deacetylation of chitin (Rinaudo, 2006). Chitosan NPs have shown promising results for oral delivery/supplementation due their GRAS properties and their intrinsic properties, including, non-immunogenic, mucoadhesion and the ability to transiently open the tight junctions of the intestinal barrier, which can help facilitate transport of macromolecules and has the potential to act as an enhancer (Chuah, Kuroiwa, Ichikawa, Kobayashi, & Nakajima, 2009; de Moura et al., 2009; Madureira,

Pereira, & Pintado, 2016). LKP NPs were produced using an ionotropic gelation technique. This technique allows the preparation of chitosan NPs in aqueous solution and avoids the use of organic solvents, high dispersion energy and harsh conditions, making the technique suitable for the inclusion of nutraceuticals (García, Forbe, & Gonzalez, 2010). In this process, a chitosan with a high degree of deacetylation is used, which increases the viscosity and results in an extended conformation with a more flexible chain because of the charge repulsion in the molecule (Franca, Freitas, & Lins, 2011). Chitosan can be ionically cross-linked by counterions, such as sodium tripolyphosphate (TPP), to form a hydrogel of microparticles, and when the relative concentrations of chitosan and these anions are appropriate, NPs may be generated (Sureshkumar, Das, Mallia, & Gupta, 2010).

The formulation of NPs from different constituent components can be troublesome, due to the different variable parameters used (concentration, temperature and pH). Empirical optimisation using Response Surface Modelling (RSM) can help to rationalise the process and has found applications in different fields, such as engineering, pharmaceutical, biomedical, environmental and epidemiological research (Singh, Singh, Saraf, & Saraf, 2011). RSM has been shown to be useful for optimisation of experimental parameters in nanoparticle formulation, and has been adopted by a number of research groups (Abdel-Hafez, Hathout, & Sammour, 2014b; Bezerra, Santelli, Oliveira, Villar, & Escaleira, 2008).

The aim of this work is to formulate and investigate the feasibility of LKP encapsulated chitosan NPs, determining the physico-chemical characteristics, stability to storage, bioactivity and low cytotoxicity properties. The formulation of the LKP NP was optimised using a RSM approach. The physico-chemical characteristics of the NPs were assessed using dynamic laser scattering, scanning electron microscopy, and Fourier transform infrared spectroscopy, with the aim of producing the optimal NPs as an oral delivery system. Accelerated thermal conditions are employed to explore the stability for future storage

conditions; particle size, polydispersity, zeta potential and bioactivity were assessed. In addition, the cytotoxicity and release profiles in simulated gastric and intestinal fluids were assessed.

2. Materials and Methods

LKP (Mw 356.47, purity = 96% according to the manufacturer's specifications) was synthesised by ChinaPeptides Co. Ltd, (Shanghai, China). CL113 (Mw = 110 kDa, deacetylation degree (DD) = 86% according to manufacturer's specifications) was obtained from Pronova Biopolymer (Norway). TPP, Angiotensin-I converting enzyme (from rabbit lung), captopril, N-α-hippuryl-L-histidyl-L-leucine hydrate salt (HHL) and all other materials were obtained from Sigma-Aldrich (Ireland). CellTitre 96® AQ_{ueous} One Solution Cell Proliferation Assay was supplied by Promega (Madison, USA). Caco-2 cells (passage 24-26) were obtained from European Collection of Cell Cultures (Salisbury, UK). HepG2 cells (passage 32-34) were obtained from American Type Culture Collection. Ultrapure water was used for all experiments and was obtained from a Milli-Q water purification system (Millipore Corporation, USA).

2.1 Unloaded nanoparticle formulation design

Unloaded NPs formulation was optimised using varying concentrations of CL113 and TPP, following a 3 block Central Composite Design (CCD) with 2 variable parameters and 3 responses (particle size, ZP and PDI).

2.2 LKP nanoparticle formulation design

A Mixture Amount Design (MAD) was employed using the concentration ranges of chitosan (CL113) and TPP (see table 1) around the optimal point (1.5mg/mL CL113 and 0.3mg/mL TPP) suggested from preliminary unloaded particle experiments (Section 3.1). The

experimental design and data analysis was performed using Minitab 17 software (Minitab Inc, USA).

Table 1 MAD for LKP nanoparticles at optimised CL113, TPP concentration

Sample	CL113 (mg/ml)	TPP (mg/ml)	Ratio (CL113/TPP)
1	1.64	0.21	8.0
2	1.52	0.33	4.5
3	1.58	0.27	5.9
4	1.45	0.40	3.6
5	1.39	0.46	3.0

2.3 Preparation of LKP NPs

Preparation of LKP NPs was based on a modified ionotropic method (Calvo, Remu, Pez, Vila-Jato, & Alonso, 1997; Vimal et al., 2013). Stock solutions of 10mg/mL CL113 and TPP were prepared. CL113 was dispersed in acetate buffer (pH3) and TPP in 0.01M sodium hydroxide solution. The stock solutions of CL113 and TPP were diluted to different concentration ratios at a fixed volume mixture of 2.5:1 CL113: TPP containing solution. A fixed concentration of 0.1mg/mL LKP was added to the diluted TPP solutions. The TPP/peptide solution was added dropwise to the CL113 solution while stirring (800rpm for 30mins). NPs were separated using ultrafiltration-centrifugation (Centriplus YM-30, MWCO of 30kDa, Millipore, USA). 10mL of sample were placed in the sample reservoir of the centrifugal filter device and centrifuged for 30mins at 3000rpm. After separation, the volume of the solution in the filtrate vial was measured and the filtrate was assayed for the amount of LKP by Reverse Phase High Performance Liquid Chromatography (RP-HPLC). The wet

pellet was re-suspended in purified water and immediately characterised using a range of physico-chemical techniques.

2.4 Physico-chemical characterisation of LKP NPs

2.4.1 Size, zeta potential and polydispersity index

The nanoparticle size (number distribution) and electrophoretic mobility measurements were performed using folded capillary cells in a Nanosizer ZS fitted with a 633 nm laser (Malvern Instruments Ltd.). Each analysis was carried out at 25°C with the equilibration time set to 2 min using size by intensity distribution.

2.4.2 Fourier transform infrared spectroscopy

The chemical properties of the NPs were monitored using Fourier transform infrared spectroscopy (FT-IR), performed using a Perkin Elmer Spotlight 400 Series Spectrometer (with Universal Attenuated total reflectance (ATR) accessory). FT-IR spectra of LKP, unloaded NPs, and LKP NPs were obtained in the spectral range 650 to 4000 cm^{-1} in triplicate. NP samples were stored at -80˚C in glass vials and then lyophilised prior to analysis using a Labconco FreeZone 6 Liter Benchtop Freeze Dry System.

2.4.3 Scanning electron microscopy

The morphology of the freeze-dried NPs was studied using scanning electron microscopy (SEM) (Hitachi SU6600 FESEM), at an accelerating voltage of 20kV using the secondary electron detector. The freeze dried NPs (0.5mg) were dispersed in deionised water (10mL) and sonicated for 4min. One drop of the dispersion containing LKP NPs was placed on a silicon wafer and dried at room temperature. This was sputter coated with 4nm Au/Pd prior to imaging.

2.4.4 Determination of association efficiency and loading capacity of LKP nanoparticles

The association efficiency (AE) and loading capacity (LC) of NPs was calculated by the indirect method of Al-Qadi *et al.* (2012). The supernatant was assayed for the content of LKP by RP-HPLC. This quantity of LKP is referred to as the non-associated peptide. The RP-HPLC analysis was performed on a Waters 1525 pump (Waters, Milford, Massachusetts) with a Photo Diode Array detector 2487 (Waters) using a Luna C18 column (5µm, 250mm x 4.6mm, Phenomenex). Analytes were detected at the wavelength of λ_{max}= 220nm. The column was eluted at a flow rate of 1mL.min^{-1} with an isocratic system (15% Acetonitrile, 0.05% TFA in water). The AE% and loading capacity (LC %) was calculated using the following equations.

$$\text{AE \%} = \frac{(\text{Total amount Peptide} - \text{free amount Peptide in supernatant})}{\text{Total amount of Peptide}} \; x\; 100 \qquad (4.1)$$

$$\text{LC\%} = \frac{(\text{Total amount Peptide} - \text{free amount Peptide in supernatant})}{\text{Nanoparticle weight}} \; x\; 100 \qquad (4.2)$$

2.4.5 ACE inhibition assay

The ACE inhibition of LKP was determined as previously described with minor modifications (Henda et al., 2013; Lahogue, Réhel, Taupin, Haras, & Allaume, 2010). All solutions were pre-filtered with 0.22µm nylon syringes prior to analysis. HHL (5mM) was dissolved in pH 8.3 buffer (0.1M borate buffer in 0.3M NaCL). In a 96-well plate, 100µl substrate solution and 25µl inhibitor were incubated for 10min at 37°C. 10µl ACE solution (100mU/mL) was then added and incubated for another 30min at 37°C. The assay was terminated using 100µ1 of 1M HCL. HPLC was performed using a C8 column (2.7µm, 3.0 x 100mm, Agilent Technologies UK & Ireland Ltd) and wavelength detection at λ_{max}= 228nm. An isocratic method was used at a flow rate of 0.4mL.min^{-1}, 25% Acetonitrile, 0.1% TFA in water for 5min. Controls were prepared by replacing the inhibitor with assay buffer (negative

control) and captopril (positive control). 100% ACE inhibition (negative control) was used to calculate the % of ACE activity.

$$ACE\ inhibition\ (\%) = \left(1 - \frac{A_{inhibitor}}{A_{blank}}\right) * 100 \quad (4.3)$$

where $A_{inhibitor}$ and A_{blank} are the peak areas of HA (product of HHL) and negative control, respectively. The IC_{50} of the inhibitor was determined using the Hill-Step equation (Prism 5, GrapPad Software Inc., USA).

2.4.6 Accelerated stability analysis

The optimal formulation was further analysed under accelerated stability conditions. 10mL of a NP formulation equivalent to 19.5mg of NPs were resuspended in aqueous solution (pH7) and stored at accelerated conditions; 60°C for 720min, 70°C for 300min and 80°C for 120min. The particle size and colloidal stability over different time intervals were measured using the Nanosizer ZS (Malvern Instruments Ltd), and the order of degradation in aqueous LKP suspension was determined. The end point of each sample was further assessed for ACE inhibition activity (Method 2.4.5). Stability analysis was analysed using R software (R Core Team, 2015).

The kinetic model used to describe the stability was of zero order. The temperature dependence of the kinetic parameters of LKP NPs stability was measured by calculating the observed rate constants. This was plotted according to the Arrhenius equation and apparent activation energy, E_a and reaction rate, k_{ref} were calculated according to Equation 4 (Brauner & Shacham, 1997).

$$C = Co + e^{\ln(k) - \frac{Ea}{R}\left(\frac{1}{T} - \frac{1}{T_{ref}}\right)t} \quad (4.4)$$

where C is the property (particle size or PDI) at time t, Co is the initial property conditions, k is the apparent zero order reaction constant, E_a is the energy of activation, R is the universal

223 gas constant, T is the temperature of the experiment (K) and T_{ref} is the reference temperature
224 (70°C).

225 2.4.7 MTS assay

226 Caco-2, heterogeneous human epithelial colorectal adenocarcinoma cells and HepG2, a
227 human liver cancer cell line, were seeded at a cell density of 2 x 10^4 cells/well and cultured
228 on 96 well plates in DMEM and EMEM respectively, supplemented with 10% fetal bovine
229 serum, 1% $_L$-glutamine, 1% penicillin-streptomycin and 1% non-essential amino acids, and
230 incubated for 24h at 37°C in a humidified incubator with 5% CO_2 and 95% O_2. Specified
231 exposure times were used for Caco-2 and HepG2, in order to mimic *in vivo* conditions. The
232 maximum time NPs will be exposed to the intestines are 4h, hence a 4h exposure time was
233 used in Caco-2 cell lines (Neves, Martins, Segundo, & Reis, 2016). In addition to this, 72h
234 exposure time was used for HepG2 cell line to mimic the liver (Brayden, Gleeson, & Walsh,
235 2014). LKP (native), unloaded NP and LKP NPs at 1, 5 and 10mM concentration were
236 assessed. Triton X-100™ (0.05%) was used as a positive control. After exposure, treatments
237 were removed and replaced with MTS (3-(4,5-dimethylthiazol-2-yl)-5-(3-carbo
238 xymethoxyphenyl)-2-(4-sulfophenyl)-2H-tetrazolium. Optical density (OD) was measured at
239 490 nm. Each value presented was normalised against untreated control and calculated from
240 three separate experiments, each of which included six replicates.

241 2.4.8 *In vitro* controlled release studies

242 LKP release from loaded formulation was carried out using a dialysis bag diffusion technique
243 (Hosseinzadeh, Atyabi, Dinarvand, & Ostad, 2012) over 24h (Calderon *et al*., 2013; Yoon *et*
244 *al*., 2014). To ensure sink conditions, NPs were solubilised and sonicated 3 times for 20
245 seconds (Branson Ultrasonics; Ultrasonic processor VCX-750W, Wilmington, North
246 Carolina, USA). 5mL of LKP formulation was placed in the dialysis bag (cellulose ester

247 membrane, molecular weight cut-off 100kDa, Float-A-Lyzer®G2, Sigma-Aldrich, Ireland)
248 and immersed in a vessel containing 50mL of release fluid using simulated gastric fluid
249 (SGF) or simulated intestinal fluid (SIF) specified according to the British Pharmacopoeia,
250 respectively. SGF was composed of 0.1 M HCL and SIF, as the buffering stage, was
251 composed of 1 volume of 0.2 M trisodium phosphate dodecahydrate and 3 volumes of 0.1 M
252 HCL (adjusted to pH 6.8), without enzymes (British Pharmacopoeia Commission, 2016).
253 Each experiment was agitated at 100rpm, 37◦C using a thermostatic shaker. At predetermined
254 time points over 24h, 1mL of release fluid was analysed and replaced with simulated fluid.
255 The LKP release was measured using RP-HPLC. The following equation was employed to
256 determine the % cumulative drug release:

257 $$\%\ \text{cumulative release} = \frac{\text{LKP release}}{\text{LKP initial}} * 100 \qquad (4.5)$$

258 where LKP release and initial represents the concentration of LKP release and the amount of
259 LKP initially loaded into the NPs, respectively.

260 **3. Results and discussion**

261 LKP has an isoelectric point (pI) of 9.17, calculated using the Henderson-Hasselbach
262 equation (Henriksson, Englund, Johansson, & Lundahl, 1995). This is the net charge of a
263 molecule indicating that, at a pH of 9.17, LKP will have minimal solubility. At pH values
264 below the pI, peptides carry a net positive charge and above the pI, a negative charge. LKP
265 has a similar charge to TPP, and hence LKP was dissolved in the TPP solution. TPP-LKP
266 was then added dropwise to the CL113 solution, resulting in the formation of opalescent NPs.

267 3.1 Unloaded nanoparticle production feasibility zone identification

268 The formulation of CL113 NPs was optimized using a CCD factorial design to analyse the
269 effect of the pH, CL113: TPP ratio and acetic acid concentration on the size and ZP of the
270 particles. Preliminary studies were conducted to select the most feasible region for the

formulation of peptide NPs (figure 1). This showed that > 1.25 mg/mL CLL113 and 0.25-0.3 mg/mL TPP resulted in unloaded NPs of optimal sizes of 300 nm and ZP > 30 mV.

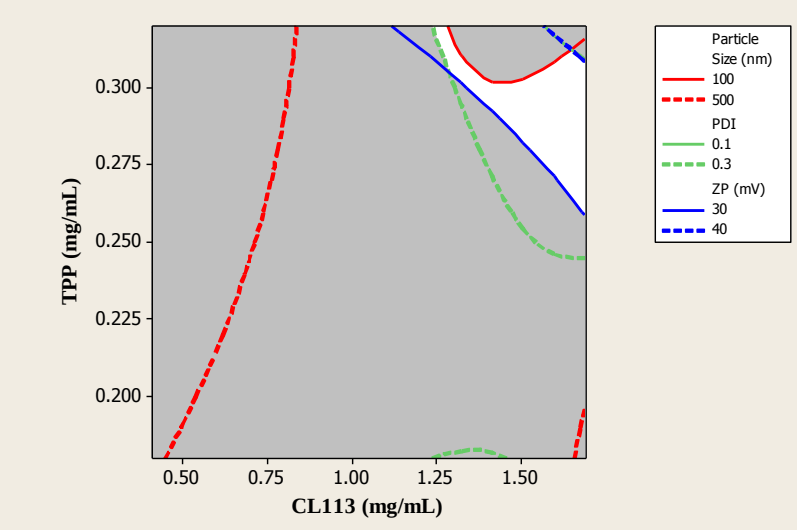

Figure 1 Overlaid contour plots of Size and ZP: the targeted area is highlighted (white).

This result is in agreement with Calvo et al., (1997) who reported that concentrations which exceed 4mg/mL and 0.75mg/mL respectively for chitosan and TPP resulted in the formation of large aggregates. Nanoparticles of the desired characteristics were found to be produced at concentrations of 0.28 mg/mL (TPP) and 1.25 mg/mL (Chitosan). In addition, studies done by de Pinho Neves et al. (2014) showed similar results within the 5 to 6:1 ratio. Unloaded CL113 NPs were used as control for peptide-loaded experiments.

3.2 Nanoparticle size, zeta potential analysis and AE % of LKP nanoparticles

From the preliminary optimisation analysis of unloaded CL113 NPs; a CL113 concentration of 1.5mg/mL was chosen as the centre point for the MAD. LKP NP size values ranged from 120 to 271nm, with ZP values above 30mV. With regards to the AE % (figure 2), at ratios above 5.9, there is less variability (error bars), but at a ratio of 8, stable agglomerates (> 30mV ZP) of variable sizes are observed.

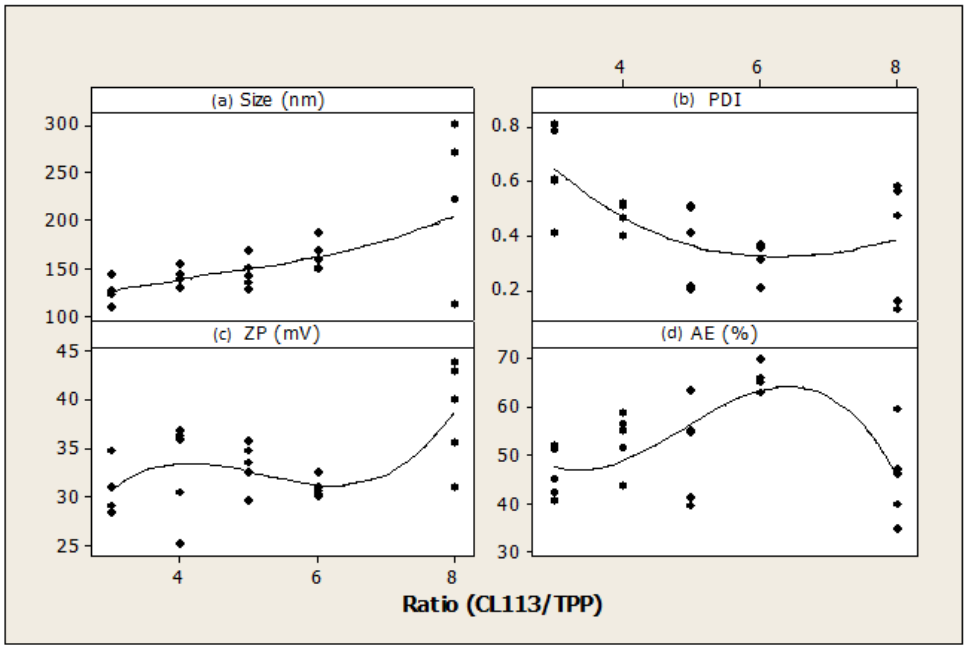

287

288 **Figure 2** Scatterplot of (a) Size (nm), (b) PDI, (c) ZP (mV) and (d) association efficiency
289 (AE %) of LKP NPs against different ratios of (CL113/ TPP). Error bars represent the
290 individual 95% Confidence interval for the average

291 An initial observation of the results at different ratios seems to indicate that the ratio of 5.9 is
292 the best performing in terms of higher AE% and lower PDI, while still maintaining a particle
293 size (150nm) and a ZP (>30mv) that indicates stability (figure 2). LC% for all experiments
294 showed no significant differences, values ranged from 2-3% (see supplementary material, S2)
295 were attained. Studies from other groups showed that an increase of counterion (TPP)
296 concentration results in a decrease of LC due to the high level of crosslinking, causing the
297 encapsulated material to come out of the particle (Woranuch & Yoksan, 2013).
298 Similar profiles are seen for the 3 responses, size (nm), ZP (mV) and PDI, suggesting
299 agglomeration and colloidal instability above a ratio (CL113/TPP) of 7. The degree of
300 crosslinking can be assessed by the chitosan concentration and the available NH3+ able to be
301 crosslinked with TPP functional groups. At intermediate operation conditions, i.e. ratios
302 between 7 and 5.5, most responses present a lower variation between replicates with respect

to all responses and a minimum PDI. Analysis for all experimental results shows particle sizes within the optimal size range (100-500nm) and ZP above 30mV values. However, for some experimental conditions, the AE% and PDI exhibited values far from the optimal physico-chemical characteristics and had high variability between replicates (N=3). At (CLL113/TPP) ratios above 7 and below 4.5, the NPs exhibited higher PDI and, below a ratio of 6, significant variability of AE% amongst replicates is evident.

The results obtained were consistent with those observed for unloaded CL113 NPs in terms of particle size, although a significant increase in colloidal stability for the loaded NPs was observed (see figure 3).

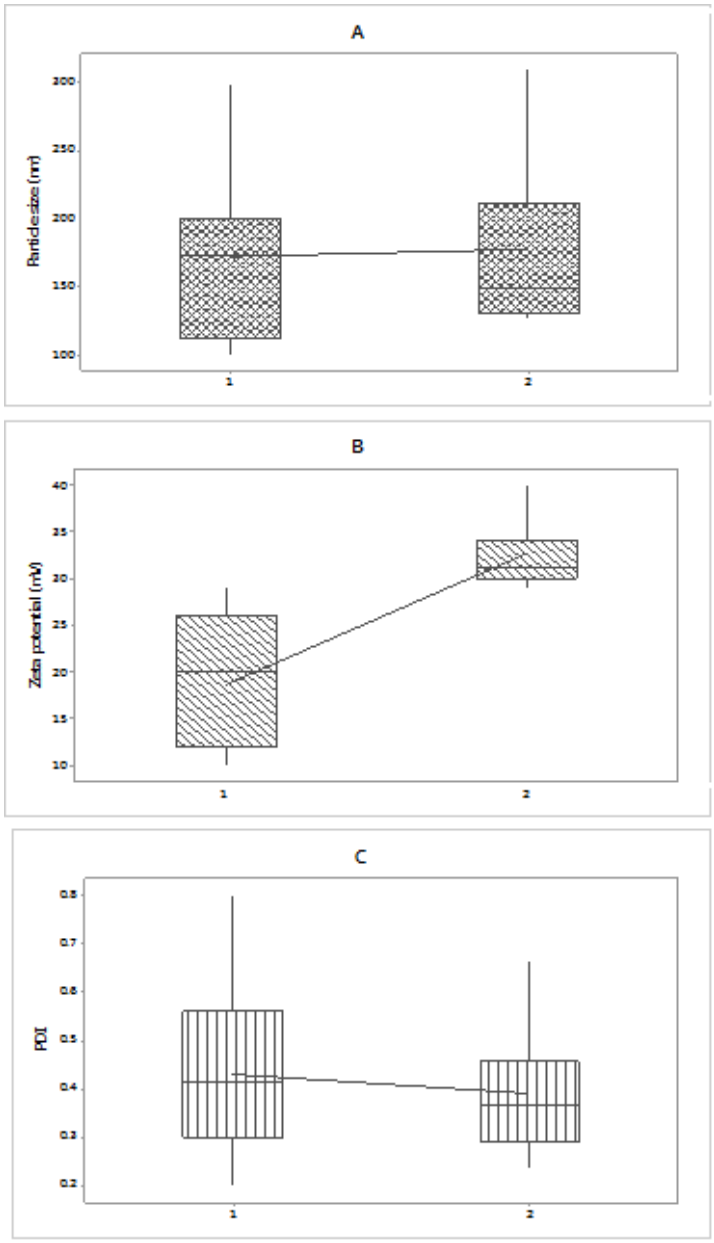

312

313 **Figure 3** Boxplot for LKP NPs where each Group represents 1: control (unloaded NPs) and
314 2: LKP NPs. The changes of each group are examined for A: particle size, B: ZP and C: PDI.
315 A significant increase in ZP is seen for loaded NPs with a decrease of variability.

316 For the MAD design, a third order polynomial regression model was employed to describe
317 the variation of size (nm), ZP (mV), PDI and AE % of the LKP NPs against the ratio
318 (CL113/TPP). The polynomial equation parameters for each response against ratio were
319 fitted. The models were built with the aim of identifying conditions within the experimental

320 design where NPs would be present as monodispersed, stable NPs with maximum peptide
321 encapsulation (see supplementary information S1).
322 From the results obtained, a ratio of 5.9 provided the most promising results, for optimal oral
323 delivery fulfilling the formulation constraints; 100-500 nm, PDI <0.4 and |ZP| >30 mV. In
324 comparison, NPs produced at a ratio of 7.8, presented the highest variability for size (206 ±
325 73 nm), PDI (0.4 ± 0.2), ZP (38 ± 6 mV) and AE (41 ± 11%). Notably, the NPs produced at a
326 ratio of 5.9 (CL113/TPP) yielded a substantially higher AE % of around 65%. It should be
327 noted that the LKP of isoelectric pH (9.17) was added to a higher pH TPP (pH 12) solution.
328 This provided more negatively charged molecules to interact with chitosan, consequently
329 increasing the AE % (Acton, 2012). This finding is in agreement with Silva et al.,(2013), who
330 observed higher AE % of daptomycin at higher pH values relative to the isoelectric pH. In
331 addition, LKP has a low Mw and studies of lower Mw actives showed higher AE %. This
332 trend was observed by Jarudilokkul et al., (2011), who showed that α-Lactalbumin (17.4 kDa)
333 has higher AE % than Fibrinogen (340 kDa).
334 3.3 Morphological characterisation of LKP chitosan nanoparticles

335 Further characterisation of the NPs produced with the optimal (CL113/TPP) ratio of 5.9 was
336 performed. Figure 4 represents an SEM image of LKP formulation, confirming the formation
337 of the NPs. Spheroidal NPs were obtained, of sizes ranging from 150-250nm, consistent with
338 the DLS measurement.

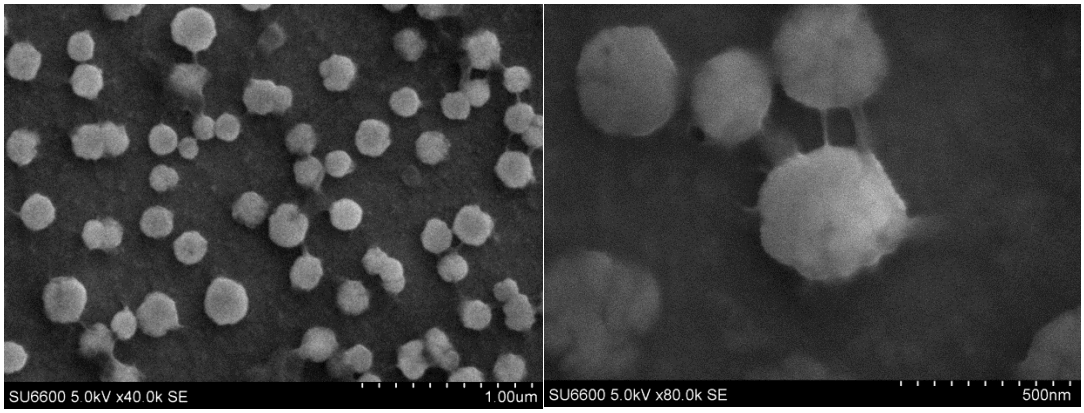

Figure 4 SEM image of optimal formulation (Ratio 5.9) of LKP NPs

3.4 Chemical Characterisation of LKP nanoparticles

FT-IR was used to identify whether there were variations in chemical functional groups presented in the LKP loaded NPs with respect to their raw materials. An FT-IR analysis was conducted for pure LKP powder, unloaded NPs and LKP NPs (Figure 5). Chitosan NPs have been previously characterised using FT-IR (Mohammadpour Dounighi et al., 2012; Sureshkumar et al., 2010; Vimal et al., 2013).

Comparison of the FT-IR spectra of loaded and unloaded NPs indicated that the spectrum of the unloaded NPs is largely unchanged by the presence of LKP, as may be expected due to the relatively low LKP content. Characteristic peaks of unloaded NPs are seen in both, at 1530, 1636 and 880cm^{-1}, representing the amide I and amide II bands of CL113 and pyranose (P-O) of TPP. For the optimal formulation, 18.5mg of NPs is needed to encapsulate 1mg of LKP. Hence, no distinctive peaks of LKP can be seen in the LKP spectrum. The FT-IR spectrum of LKP NPs does, however, show some changes from that of the unloaded NPs, potentially indicative of localised conformational changes of the CL113 as a result of interaction with the LKP (figure 5). An increased absorption at 3386cm^{-1} compared to that of the unloaded NPs is observed. Absorption in this region of the spectrum represents O-H bonding; a possible explanation may be due to the interaction of the hydrogen acceptors (O-

in LKP) and hydrogen donors (NH_3+ in chitosan). In addition, increased absorption is also seen for LKP NPs at 2955cm^{-1}, representing an increase in (C-H) hydrogen bond stretching with presence of the peptide. A shift of 1605cm^{-1} to 1530cm^{-1} was also observed which represent the amide carbonyl stretch (Mohammadpour Dounighi et al., 2012). The peaks at 1210cm^{-1} and 880cm^{-1} represent phosphate group (P-O) and pyranose ring (Woranuch & Yoksan, 2013). The peak at 1051cm^{-1} shows a split for the loaded NPs, suggesting a conformational change due to the interaction with the LKP.

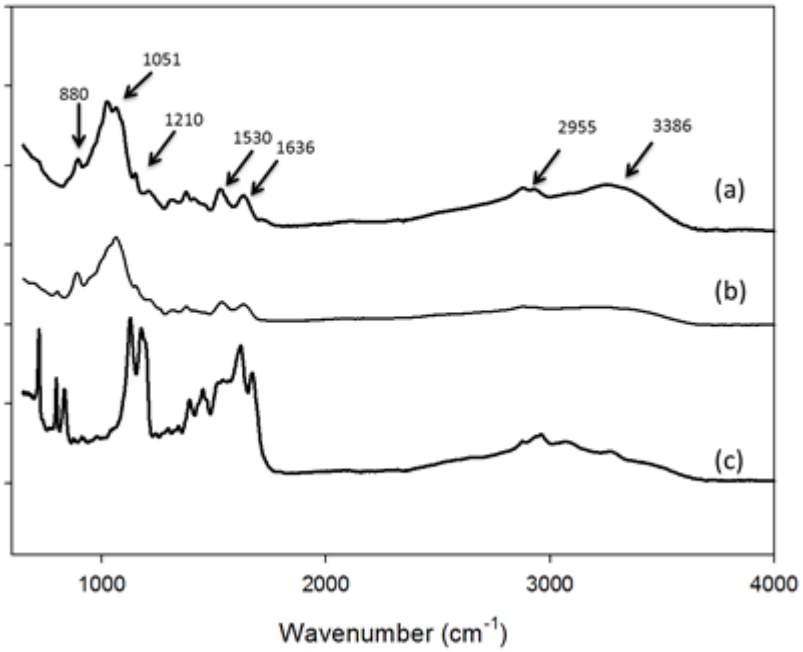

Figure 5 FT-IR spectra of (a) LKP NPs (b) unloaded NPs and (c) Pure LKP powder. Absorbance spectra are normalised and offset for clarity.

3.5 IC_{50} determination of inhibitor

The inhibitory activities of captopril (reference molecule) and LKP were determined using a synthetic substrate, HHL, and varying concentrations over the range 0.0001 – 10µM (captopril) and 0.001 - 10µM (LKP). The IC_{50} obtained was 0.006 ± 0.002 µM for captopril and 0.30 ± 0.08 µM for LKP. These values are consistent with previously reported values,

which range from 0.001-0.039µM for Captopril and 0.2-0.32µM for LKP (Fujita & Yoshikawa 1999; Fujita *et al*. 2000; Henda *et al*. 2013).

3.6 Accelerated stability analysis of LKP NPs

In accelerated stability testing, a product is stressed at high temperatures and degradation/stability of the product at normal storage conditions is then predicted (Bajaj, Singla, & Sakhuja, 2012; Rauk, Guo, Hu, Cahya, & Weiss, 2014; Waterman & Adami, 2005). A number of factors can affect the solution stability of NPs, for example, the pH of the aqueous solvents, light, oxygen, co-solutes, buffer salts, surfactants and antioxidants. Common degradation routes include hydrolysis/solvolysis, photolysis/oxidation and racemisation (Weber, Coester, Kreuter, & Langer, 2000). A number of groups have found that CL113 NPs synthesised by ionic gelation lose their integrity in aqueous media, even in the absence of enzymes (López-León, Carvalho, Seijo, Ortega-Vinuesa, & Bastos-González, 2005). Jonassen *et al.* (2012) looked at the effect of different ionic strength over the course of a month; the main findings were that the most stable NPs with respect to the size and compactness of the particles were produced in saline conditions (Jonassen, Kjøniksen, & Hiorth, 2012). A similar study was also conducted, preparing NPs in different ionic strength and buffers, and results showed that the least stable NPs were produced in non-buffered solutions or low ionic solutions (López-León et al., 2005).

The stability of formulations can be tested using a number of testing protocols, which include real time stability testing, accelerated stability testing, retained sample stability testing and cyclic temperature stress testing (Bajaj et al., 2012). In the current study, accelerated stability testing was used, by which NPs are subjected to stress and then assayed simultaneously to predict the likelihood of instability based upon the Arrhenius equation. Suspensions of NPs in buffered solutions (PBS pH 7), formulated at a ratio of 5.9 CL113:TPP (optimal LKP loaded

NPs), were exposed to three different storage temperatures, 60°C, 70°C and 80°C, over a time course of 120, 300 and 720min at each temperature. Figure 6 shows the kinetic behaviour of the particle sizes at different temperatures. The stability of the NPs decreased with increasing temperature. At 60°C, no change in particle size was observed over the 720min. Figure 6 indicates a more pronounced increase in both particle size and PDI at 70°C, while at 80°C, both particle size and PDI increase significantly over the time course. At this temperature, the particle size was seen to increase monotonically from 200 to 600nm, while the PDI increases from 0.4 to 0.7. While some curvature is apparent in the trends at the highest temperature, within the present experimental error, an apparent zero order mechanism fitted better to all the data, compared to an apparent first or second order model.

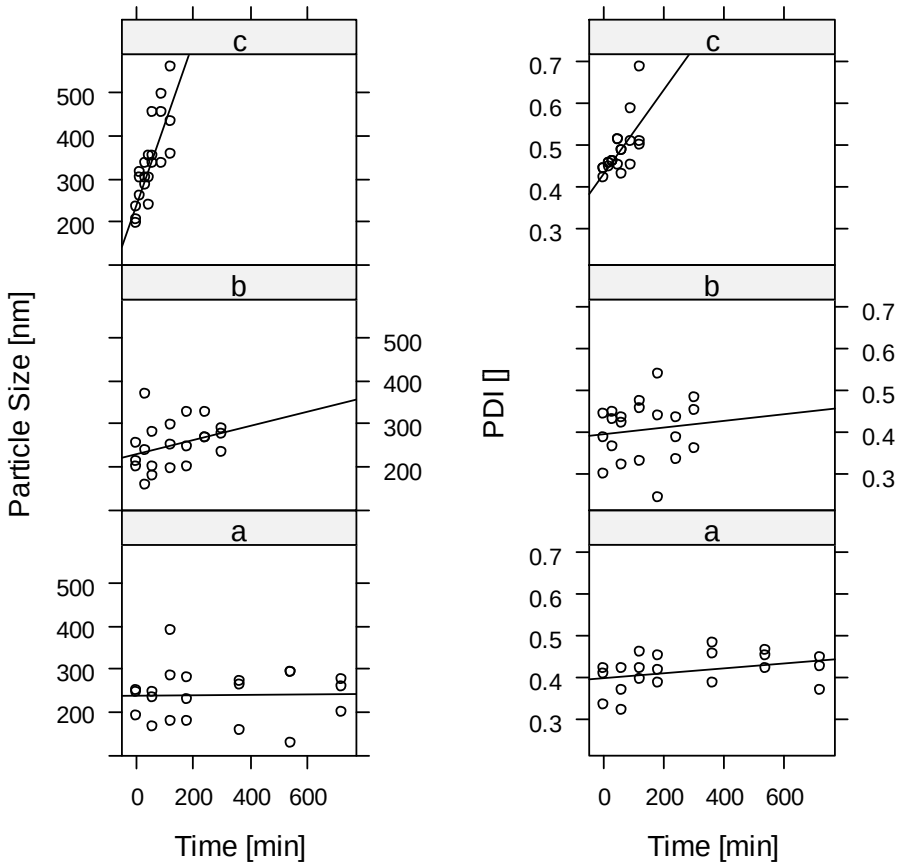

407

408 **Figure 6** Particle size and PDI analysis of LKP loaded NPs exposed at (a) 60°C (b) 70°C and
409 (c) 80°C over time periods of 120, 300 and 720min, respectively. N= 3

410 An Arrhenius plot of the apparent zero order reaction rate constants, derived from the
411 analysis of the individual experiments at the different temperatures, indicates that the kinetics
412 of the particle size and PDI followed this temperature relationship, consistent with an energy
413 activated process, with similar energies of activation for particle size and PDI (see Figure 7).

414 The one-step nonlinear regression analysis of the kinetic experiments shows that the particle
415 size fits to a zero order kinetic behaviour and an Arrhenius dependence with ln ($k_{ref@70C}$) = -
416 3±1 min^{-1} and an E_a of = 360±103 kJ/mol. For the PDI, a one-step nonlinear regression was
417 fitted to zero order kinetics with an Arrhenius dependence of ln (k_{ref}@70°C) = -8.9± 0.3$mins^{-1}$
418 and E_a =196± 33 kJ/mol. A linear correlation is evident between 1/T and ln k in figure 7.

From this analysis, it suggests the nanoparticle formulation would be stable (in terms of particle physico-chemical properties) in a neutral pH solution at ambient storage temperature, with negligible increases in particle size or PDI of the NPs, confirming the higher stability of NPs prepared in buffered solutions. Only after 90min destabilisation of NPs was observed at the highest temperature conditions. These results are in agreement with previous literature, reporting that when NPs are produced in salt or buffered environment, stability is improved (López-León et al., 2005).

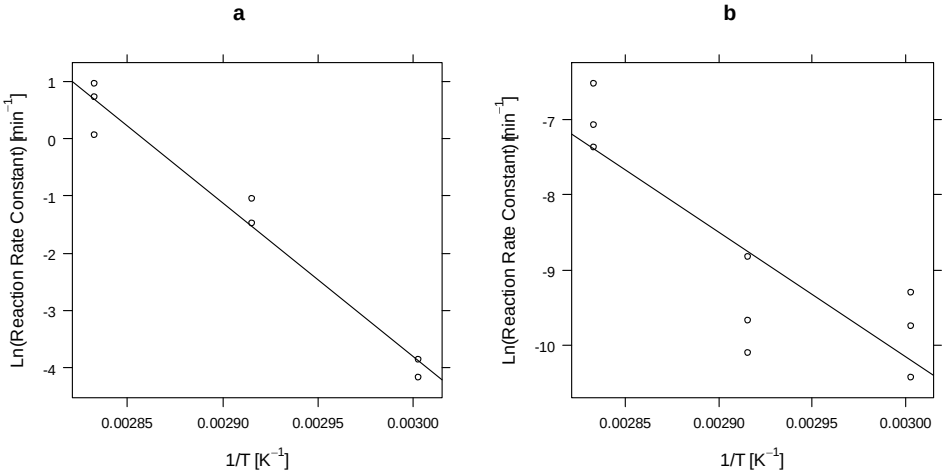

Figure 7 Arrhenius Plots for the (a) Particle Size and (b) PDI accelerated studies of LKP loaded NPs. N=3

The results suggest either (i) swelling of the chitosan NPs in the aqueous environment (Bajpai & Maan, 2012) or (ii) agglomeration of chitosan NPs due to electrostatic interactions with an increase of temperature. In order to confirm the type of degradation, the zeta potential was assessed**.** Destabilisation of NP suspensions which would give rise to aggregation should be reflected in changes in ZP values when NPs aggregate. However, no significant changes were seen for the colloidal stability (i.e. ZP of LKP NPs). This suggests that swelling could be the primary mechanism of the CL113 nanoparticle changes with time, followed by destabilisation at higher temperatures and longer time (see figure 8).

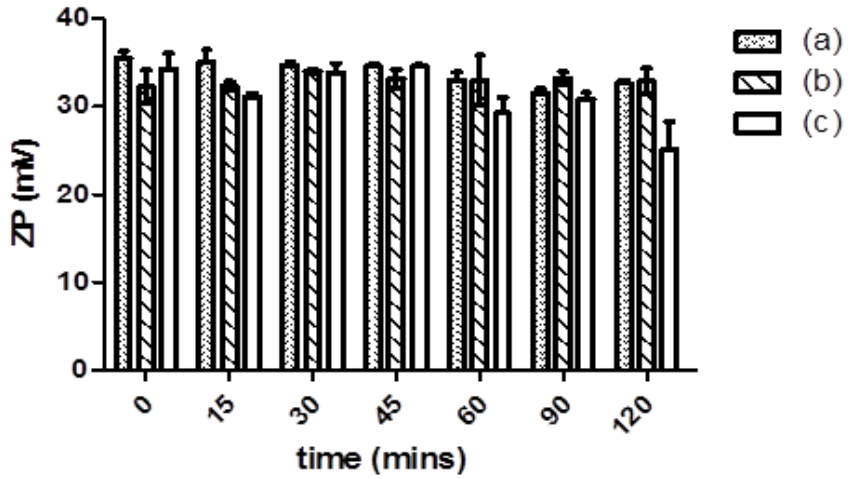

Figure 8 Zeta potential analyses of LKP-loaded NPs at (a) 60°C, (b) 70°C and (c) 80°C. No significant changes were observed with One-Way ANOVA with Dunnetts's post-test. Each value represents the mean ± SD (n=3)

In addition, DD of CL113 used for this experiment is greater than 85%, it has been previously reported that with an increase of DD the aggregation stability decreases due to the CL113 more prone to TPP bridging which causes it to become more lyophobic near physiological pH which may contribute to the stability of the NPs (Haung, Cai, & Lapitsky, 2015). Overall, the accelerated experiments on LKP NPs indicate that the formulations will be stable under normal storage conditions. This could be due to the conditions (presence of salt) used to prepare the NPs, in addition to the strong bonding between the bioactive and complex.

3.7 Cytotoxicity assessment of LKP nanoparticles

The MTS assay was used to assess the cytotoxicity of LKP and LKP NPs. The therapeutic dose of LKP is 10mg/kg (Fujita et al., 2000; Fujita & Yoshikawa, 1999b). Hence, LKP loaded or unloaded NPs at the different concentrations (1, 5 and 10mM) when exposed to Caco2 (4h) and HepG2 (72h) cell lines. No cytotoxicity was observed for LKP, indicating

negligible overall cytotoxicity of the formulation (figure 9). No significant changes were observed. A number of deviations were observed above 100% viability for NPs with and without LKP, proliferation may occur due to increase in fibroblasts production caused by the presence of polymeric chitosan (Rajam, Pulavendran, Rose, & Mandal, 2011) or interference of NPs with the cell assay (Casey et al., 2007).

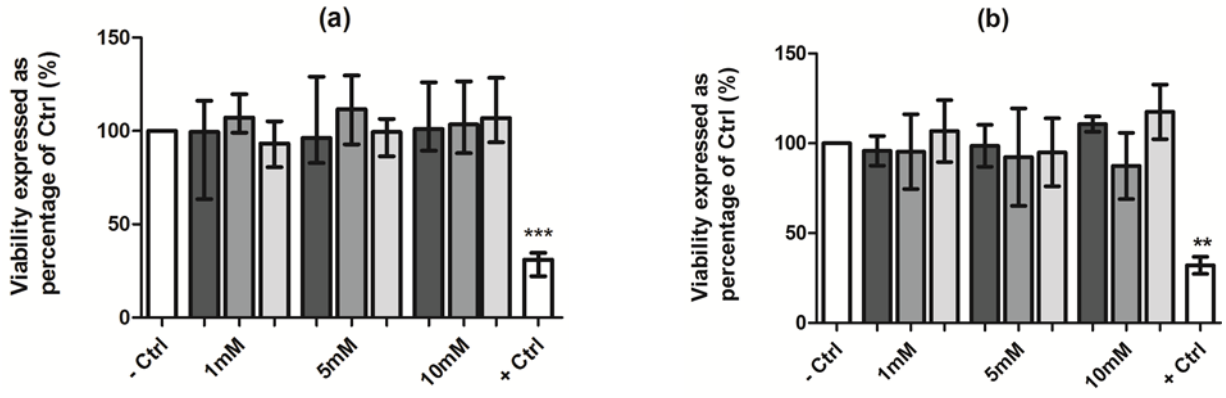

Figure 9 Cytotoxicity assessment of ■ LKP, ▭ unloaded NPs and ▭ LKP NPs exposed for (a) 4h in Caco2 cell lines and (b) 72h in HepG2 cell line at 1mM, 5mM and 10mM concentration. Percentage (%) of MTS converted was compared to untreated control. 1-Way ANOVA with Dunnetts's post-test *** P< 0.001, ** P< 0.01, N=3

3.8 *In vitro* release studies

The release of a bioactive can take place by several different mechanisms, for example surface erosion, disintegration, diffusion and desorption (Hosseini, Zandi, Rezaei, & Farahmandghavi, 2013). Such a phenomenon can be influenced by a number of factors such as the type of polymer used, the polymeric swelling capability, the solute diffusion and material degradation (Fu & Kao, 2009; Siepmann & Göpferich, 2001). The *in vitro* LKP release profiles of the NP formulation in SGF and SIF were measured over 24h, using RP-HPLC at 220nm at different time points. The site of target for LKP is in the jejunum, small

intestine, therefore it is important to bypass the acidic stomach environment. LKP NPs results showed an initial burst followed by a slow release. Similar results were reported by other groups, Hosseini *et al.* 2013 and Luo *et al*. 2010. Hosseini *et al*. 2013, they observed a "biphasic release" mechanism (initial burst followed by slower release) with oregano essential oil when encapsulated into CL113 NPs. Luo *et al*. 2010, encapsulated selenite in chitosan NPs, demonstrating the effect of CL113 concentration on the release profile. They found that, at high concentrations of chitosan, more dense particles were found which ultimately lowered the epithelial membrane permeability. Conflicting results have been reported of the release mechanism of chitosan nanoparticles. Some groups observed the inability of chitosan based nanoparticles to sustain the release of an active following an initial burst release at higher ratios of CL113 and TPP (Stoica & Ion, 2013). Others reported a controlled release; for example, Nallamuthu, Devi, & Khanum, (2015) observed the 69% release of chlorogenic acid over 100 h. Release profiles at 1.5mg/ml CL113 also showed a burst within the first 30min in the SGF followed by a slower release from 30min to 2h then a more slow sustained release up to 24h, as shown in figure 10. For LKP NPs, the initial burst may possibly represent loosely bound LKP around the CL113 NP. Within the first hour, 62% ±3 and 74% ±4 LKP was released in (a) SGF and (b) SIF, significance was observed for SGF vs SIF using a t-test, where $P = 0.0074$, respectively (figure 10). 12% more release was observed in the SIF (site of target) at pH 6.8. Chitosan has an isoelectric point of 6.5, at which pH chitosan holds a charge of zero (no charge), causing it to become unstable and precipitate out; consequently releasing more of the loaded peptide. It has been suggested by Gan & Wang, (2007) that a burst release of protein molecules may correspond to the fast swelling and degradation of the nanoparticles. This swelling phenomenon can be observed in (figure 10) After 1h, a slower release is observed, this may be attributed to the more strongly bound LKP loaded within the CL113 nanoparticle. A burst release has previously been

reported from other groups working with chitosan NPs, Sarmento *et al.* (2007) showed a similar undesirable burst of 50% insulin chitosan NPs when complexed with alginate. Ryan *et al.* (2013) also reported an initial burst of 40% of salmon calcitonin when complexed into a NPs system using chitosan and hyaluronic acid. For oral delivery systems, NPs remain in the system for up to 6h after intake. Our studies show after 6h up to 85% release was obtained. However, a prolonged release is desired. Additional of an outer surface coating is a technique which has been widely used by a number of researchers in order to improve the integrity of the NPs and to better control the release profile (Elgadir et al., 2015). A popular approach to yield coated chitosan NPs is by polyelectrolyte complexation, which exploits the interaction between positively charged chitosan and negatively charged polyelectrolytes such as alginate (Garrait, Beyssac and Subirade, 2014), dextran (Sarmento et al., 2006), hyaluronic acid (Mero et al., 2014) or zein (Luo, Teng and Wang, 2012). Further work on LKP encapsulation will involve the polyelectrolyte complexation of LKP to achieve the desired release.

.

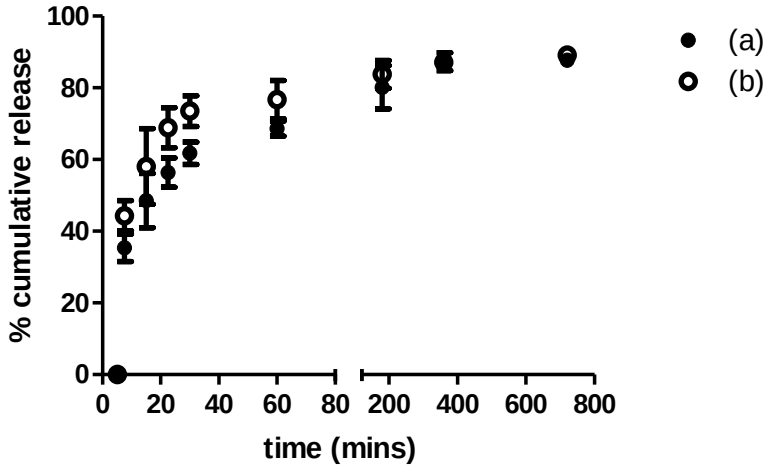

Figure 10 Cumulative release profile of LKP from NPs in (a) SGF and (b) SIF for 24h.

4. Conclusions

LKP loaded NPs were formulated successfully by applying the ionotropic gelation technique. The optimal NPs were found at a ratio 5.9:1 (CL113: TPP), using the design of experiment approach, which resulted in reproducibility of the desirable physico-chemical characteristics. Optimally LKP NPs were spheroidal particles of size ~200nm, as shown by SEM, and had enhanced colloidal stability compared to the unloaded particles. A 5.9:1 ratio provided high encapsulation efficiency of 65±3% with loading capacity of approximately 5±0.8 %. Stability analysis showed long term physico-chemical stability. ACE inhibitory studies presented no change in bioactivity of LKP over the different temperature conditions and after formulation indicating it is quite stable. In addition, no cytotoxicity was observed from both the LKP loaded and unloaded NPs. *In vitro* release studies indicated an initial burst within 1h, suggesting the presence of more loosely bound tripeptide in the nanoparticle complex, followed by peptide bounded within the nanoparticle which is released at a slower rate. Chitosan based delivery systems is a feasible for the formulation of bioactive peptide, physicochemical analysis and stability was efficient. The present results indicate that the addition of an enteric coating to is recommended in order to bypass the stomach acidic pH conditions, providing am efficient delivery system.

Acknowledgements

This project is funded by an Irish Department of Agriculture Food Institutional Research Measure (FIRM) grant 'NUTRADEL' grant number 11F042. Special thanks to Dr Anne Shanahan for the assistance in image analysis.

References

Abdel-Hafez, S. M., Hathout, R. M., & Sammour, O. a. (2014a). Towards better modeling of chitosan nanoparticles production: Screening different factors and comparing two

experimental designs. *International Journal of Biological Macromolecules*, *64*, 334–340. http://doi.org/10.1016/j.ijbiomac.2013.11.041

Abdel-Hafez, S. M., Hathout, R. M., & Sammour, O. a. (2014b). Towards better modeling of chitosan nanoparticles production: Screening different factors and comparing two experimental designs. *International Journal of Biological Macromolecules*, *64*, 334–340. http://doi.org/10.1016/j.ijbiomac.2013.11.041

Acton, Q. A. (2012). *Advances in Nanotechnology Research and Application: 2012 Edition*. ScholarlyEditions. Retrieved from https://books.google.ie/books?id=jYeUaTkR9P8C

Bajaj, S., Singla, D., & Sakhuja, N. (2012). Stability testing of pharmaceutical products. *Journal of Applied Pharmaceutical Science*, *2*(3), 129–138. http://doi.org/10.7324/JAPS.2012.2322

Bajpai, J., & Maan, G. K. (2012). Preparation , Characterization and Water Uptake Behavior of Polysaccharide Based Nanoparticles Swelling behavior of nanoparticles. *Progresses in Nanotechnology and Nanomaterials*, *1*(1), 9–17.

Berilyn, P., So, T., Rubio, P., Lirio, S., Macabeo, A. P., Huang, H.-Y., … Villaflores, O. B. (2016). In vitro angiotensin I converting enzyme inhibition by a peptide isolated from Chiropsalmus quadrigatus Haeckel (box jellyfish) venom hydrolysate. *Toxicon : Official Journal of the International Society on Toxinology*, *119*, 77–83. http://doi.org/10.1016/j.toxicon.2016.04.050

Bezerra, M. A., Santelli, R. E., Oliveira, E. P., Villar, L. S., & Escaleira, L. a. (2008). Response surface methodology (RSM) as a tool for optimization in analytical chemistry. *Talanta*, *76*(5), 965–977. http://doi.org/10.1016/j.talanta.2008.05.019

561 Bougatef, A., Nedjar-Arroume, N., Ravallec-Plé, R., Leroy, Y., Guillochon, D., Barkia, A., &
562 Nasri, M. (2008). Angiotensin I-converting enzyme (ACE) inhibitory activities of
563 sardinelle (Sardinella aurita) by-products protein hydrolysates obtained by treatment
564 with microbial and visceral fish serine proteases. *Food Chemistry*, *111*(2), 350–356.
565 http://doi.org/10.1016/j.foodchem.2008.03.074

566 Braithwaite, M. C., Tyagi, C., Tomar, L. K., Kumar, P., Choonara, Y. E., & Pillay, V. (2014).
567 Nutraceutical-based therapeutics and formulation strategies augmenting their efficiency
568 to complement modern medicine: An overview. *Journal of Functional Foods*.
569 http://doi.org/10.1016/j.jff.2013.09.022

570 Brauner, N., & Shacham, M. (1997). Statistical analysis of linear and nonlinear correlation of
571 the Arrhenius equation constants. *Chemical Engineering and Processing: Process*
572 *Intensification*, *36*(3), 243–249. http://doi.org/10.1016/S0255-2701(96)04186-4

573 Brayden, D. J., Gleeson, J., & Walsh, E. G. (2014). A head-to-head multi-parametric high
574 content analysis of a series of medium chain fatty acid intestinal permeation enhancers
575 in Caco-2 cells. *European Journal of Pharmaceutics and Biopharmaceutics*, *88*(3), 830–
576 839. http://doi.org/10.1016/j.ejpb.2014.10.008

577 British Pharmacopoeia Commission. (2016). *British Pharmacopoeia: Appendix XII B.*
578 *Dissolution*. London: TSO.

579 Bruno, B. J., Miller, G. D., & Lim, C. S. (2013). Basics and recent advances in peptide and
580 protein drug delivery. *Therapeutic Delivery*, *4*(11), 1443–67.
581 http://doi.org/10.4155/tde.13.104

582 Calderon L., Harris, R., Cordoba-Diaz, M., Elorza, M., Elorza, B., Lenoir, J., … Cordoba-
583 Diaz, D. (2013). Nano and microparticulate chitosan-based systems for antiviral topical

584 delivery. *European Journal of Pharmaceutical Sciences*, *48*, 216–222.
585 http://doi.org/10.1016/j.ejps.2012.11.002

586 Calvo, P., Remu, C., Pez, N.-L., Vila-Jato, J. L., & Alonso, M. J. (1997). Novel Hydrophilic
587 Chitosan–Polyethylene Oxide Nanoparticles as Protein Carriers. *Jounal of Applied*
588 *Polymer Science*, *63*(1), 125–132. http://doi.org/10.1002/(SICI)1097-
589 4628(19970103)63:1<125::AID-APP13>3.0.CO;2-4

590 Calvo, P., Remunan-Lopez, C., Vila-Jato, J. L., & Alonso, M. J. (1997). Novel hydrophilic
591 chitosan-polyethylene oxide nanoparticles as protein carriers. *Journal of Applied*
592 *Polymer Science*, *63*(1), 125–132.

593 Casey, A., Herzog, E., Davoren, M., Lyng, F. M., Byrne, H. J., & Chambers, G. (2007).
594 Spectroscopic analysis confirms the interactions between single walled carbon
595 nanotubes and various dyes commonly used to assess cytotoxicity. *Carbon*, *45*(7), 1425–
596 1432. http://doi.org/10.1016/j.carbon.2007.03.033

597 Choonara, B. F., Choonara, Y. E., Kumar, P., Bijukumar, D., du Toit, L. C., & Pillay, V.
598 (2014). A review of advanced oral drug delivery technologies facilitating the protection
599 and absorption of protein and peptide molecules. *Biotechnology Advances*, *32*(7), 1269–
600 1282. http://doi.org/10.1016/j.biotechadv.2014.07.006

601 Chuah, A. M., Kuroiwa, T., Ichikawa, S., Kobayashi, I., & Nakajima, M. (2009). Formation
602 of biocompatible nanoparticles via the self-assembly of chitosan and modified lecithin.
603 *Journal of Food Science*, *74*(1). http://doi.org/10.1111/j.1750-3841.2008.00985.x

604 de Moura, M. R., Aouada, F. A., Avena-Bustillos, R. J., McHugh, T. H., Krochta, J. M., &
605 Mattoso, L. H. C. (2009). Improved barrier and mechanical properties of novel
606 hydroxypropyl methylcellulose edible films with chitosan/tripolyphosphate

nanoparticles. *Journal of Food Engineering*, *92*(4), 448–453. http://doi.org/10.1016/j.jfoodeng.2008.12.015

de Pinho Neves, A. L., Milioli, C. C., Müller, L., Riella, H. G., Kuhnen, N. C., & Stulzer, H. K. (2014). Factorial design as tool in chitosan nanoparticles development by ionic gelation technique. *Colloids and Surfaces A: Physicochemical and Engineering Aspects*, *445*(2014), 34–39. http://doi.org/10.1016/j.colsurfa.2013.12.058

des Rieux, A., Fievez, V., Garinot, M., Schneider, Y. J., & Préat, V. (2006). Nanoparticles as potential oral delivery systems of proteins and vaccines: A mechanistic approach. *Journal of Controlled Release*. http://doi.org/10.1016/j.jconrel.2006.08.013

Franca, E. F., Freitas, L. C. G., & Lins, R. D. (2011). Chitosan molecular structure as a function of N-acetylation. *Biopolymers*, *95*(7), 448–460. http://doi.org/10.1002/bip.21602

Fu, Y., & Kao, W. J. (2009). Drug release kinetics and transport mechanisms from semi-interpenetrating networks of gelatin and poly(ethylene glycol) diacrylate. *Pharmaceutical Research*, *26*(9), 2115–2124. http://doi.org/10.1007/s11095-009-9923-1

Fujita, H., & Yoshikawa, M. (1999a). LKPNM: A prodrug-type ACE-inhibitory peptide derived from fish protein. *Immunopharmacology*, *44*(1–2), 123–127. http://doi.org/10.1016/S0162-3109(99)00118-6

Fujita, Yokoyama, Yoshikawa, M., Iroyukifujita, H., & Eiichiyokoyama, K. (2000). Classification and Antihypertensive Activity of Angiotensin I-Converting Enzyme Inhibitory Peptides Derived from Food Proteins. *Journal of Food Science*, *65*(4), 564–569. http://doi.org/10.1111/j.1365-2621.2000.tb16049.x

629 Fujita, & Yoshikawa, M. (1999b). LKPNM: A prodrug-type ACE-inhibitory peptide derived
630 from fish protein. *Immunopharmacology*, *44*(1–2), 123–127.
631 http://doi.org/10.1016/S0162-3109(99)00118-6

632 García, M., Forbe, T., & Gonzalez, E. (2010). Potential applications of nanotechnology in the
633 agro-food sector. *Ciência E Tecnologia de Alimentos*, *30*(3), 573–581.
634 http://doi.org/10.1590/S0101-20612010000300002

635 Gleeson, J. P., Heade, J., Ryan, S. M. M., & Brayden, D. J. (2015). Stability, toxicity and
636 intestinal permeation enhancement of two food-derived antihypertensive tripeptides, Ile-
637 Pro-Pro and Leu-Lys-Pro. TL - 71. *Peptides*, *71 VN-r*, 1–7.
638 http://doi.org/10.1016/j.peptides.2015.05.009

639 Haung, Y., Cai, Y., & Lapitsky, Y. (2015). Factors Affecting the Stability of
640 Chitosan/Tripolyphosphate Micro- and Nanogels: Resolving the Opposing Findings. *J.*
641 *Mater. Chem. B*, *3*, 5957–5970. http://doi.org/10.1039/C5TB00431D

642 Henda, Y. Ben, Labidi, A., Arnaudin, I., Bridiau, N., Delatouche, R., Maugard, T., …
643 Bordenave-Juchereau, S. (2013). Measuring angiotensin-I converting enzyme inhibitory
644 activity by micro plate assays: Comparison using marine cryptides and tentative
645 threshold determinations with captopril and losartan. *Journal of Agricultural and Food*
646 *Chemistry*, *61*, 10685–10690. http://doi.org/10.1021/jf403004e

647 Henriksson, G., Englund, A.-K., Johansson, G., & Lundahl, P. (1995). Calculation of the
648 isoelectric points of native proteins with spreading of pKa values. *Electrophoresis*,
649 *16*(1), 1377–1380. http://doi.org/10.1002/elps.11501601227

650 Hosseini, S. F., Zandi, M., Rezaei, M., & Farahmandghavi, F. (2013). Two-step method for
651 encapsulation of oregano essential oil in chitosan nanoparticles: Preparation,

652 characterization and in vitro release study. *Carbohydrate Polymers*, *95*(1), 50–56.
653 http://doi.org/10.1016/j.carbpol.2013.02.031

654 Hosseinzadeh, H., Atyabi, F., Dinarvand, R., & Ostad, S. N. (2012). Chitosan-Pluronic
655 nanoparticles as oral delivery of anticancer gemcitabine: Preparation and in vitro study.
656 *International Journal of Nanomedicine*, *7*, 1851–1863.
657 http://doi.org/10.2147/IJN.S26365

658 Jarudilokkul, S., Tongthammachat, A., & Boonamnuayvittaya, V. (2011). Preparation of
659 chitosan nanoparticles for encapsulation and release of protein. *Korean Journal of*
660 *Chemical Engineering*, *28*(5), 1247–1251. http://doi.org/10.1007/s11814-010-0485-z

661 Jonassen, H., Kjøniksen, A. L., & Hiorth, M. (2012). Stability of chitosan nanoparticles
662 cross-linked with tripolyphosphate. *Biomacromolecules*, *13*(11), 3747–3756.
663 http://doi.org/10.1021/bm301207a

664 Lahogue, V., Réhel, K., Taupin, L., Haras, D., & Allaume, P. (2010). A HPLC-UV method
665 for the determination of angiotensin I-converting enzyme (ACE) inhibitory activity.
666 *Food Chemistry*, *118*(3), 870–875. http://doi.org/10.1016/j.foodchem.2009.05.080

667 Lakshmi, P., & Kumar, G. A. (2010). Nanosuspension technology: A review. *International*
668 *Journal of Pharmacy and Pharmaceutical Sciences*.
669 http://doi.org/10.2174/092986652166614080711424O

670 Li, Y., Sadiq, F., Fu, L., Zhu, H., Zhong, M., & Sohail, M. (2016). Identification of
671 Angiotensin I-Converting Enzyme Inhibitory Peptides Derived from Enzymatic
672 Hydrolysates of Razor Clam Sinonovacula constricta. *Marine Drugs*, *14*(6), 110.
673 http://doi.org/10.3390/md14060110

López-León, T., Carvalho, E. L. S., Seijo, B., Ortega-Vinuesa, J. L., & Bastos-González, D. (2005). Physicochemical characterization of chitosan nanoparticles: electrokinetic and stability behavior. *Journal of Colloid and Interface Science*, *283*(2), 344–351. http://doi.org/10.1016/j.jcis.2004.08.186

Luo, Y., Zhang, B., Cheng, W. H., & Wang, Q. (2010). Preparation, characterization and evaluation of selenite-loaded chitosan/TPP nanoparticles with or without zein coating. *Carbohydrate Polymers*, *82*(3), 942–951. http://doi.org/10.1016/j.carbpol.2010.06.029

Ma, G. (2014). Microencapsulation of protein drugs for drug delivery: Strategy, preparation, and applications. *Journal of Controlled Release*, *193*, 324–340. http://doi.org/10.1016/j.jconrel.2014.09.003

Madureira, A. R., Pereira, A., & Pintado, M. (2016). Chitosan nanoparticles loaded with 2,5-dihydroxybenzoic acid and protocatechuic acid: Properties and digestion. *Journal of Food Engineering*, *174*, 8–14. http://doi.org/10.1016/j.jfoodeng.2015.11.007

Mohammadpour Dounighi, N., Eskandari, R., Avadi, M. R., Zolfagharian, H., Mir Mohammad Sadeghi, A., & Rezayat, M. (2012). Preparation and in vitro characterization of chitosan nanoparticles containing Mesobuthus eupeus scorpion venom as an antigen delivery system. *Journal of Venomous Animals and Toxins Including Tropical Diseases*, *18*(1), 44–52. Retrieved from http://www.scopus.com/inward/record.url?eid=2-s2.0-84859077437&partnerID=40&md5=781a81bf61973593aac773cb8b03e495

Nallamuthu, I., Devi, A., & Khanum, F. (2015). Chlorogenic acid loaded chitosan nanoparticles with sustained release property, retained antioxidant activity and enhanced bioavailability. *Asian Journal of Pharmaceutical Sciences*, *10*(3), 203–211.

http://doi.org/10.1016/j.ajps.2014.09.005

Neves, A. R., Martins, S., Segundo, M. A., & Reis, S. (2016). Nanoscale delivery of resveratrol towards enhancement of supplements and nutraceuticals. *Nutrients*, *8*(3), 1–14. http://doi.org/10.3390/nu8030131

Patel, A., Patel, M., Yang, X., & Mitra, A. K. (2014). Recent advances in protein and peptide drug delivery: a special emphasis on polymeric nanoparticles. *Protein and Peptide Letters*, *21*(11), 1102.

Quiñones, M., Margalef, M., Arola-Arnal, A., Muguerza, B., Miguel, M., & Aleixandre, A. (2015). The blood pressure effect and related plasma levels of flavan-3-ols in spontaneously hypertensive rats. *Food & Function*, *6*(11), 3479–89. http://doi.org/10.1039/c5fo00547g

R Core Team. (2015). R: A language and environment for statistical computing. R Foundation for Statistical Computing. Austria,Vienna: R Foundation for Statistical Computing,. Retrieved from http://www.r-project.org/

Rajam, M., Pulavendran, S., Rose, C., & Mandal, A. B. (2011). Chitosan nanoparticles as a dual growth factor delivery system for tissue engineering applications. *International Journal of Pharmaceutics*, *410*(1–2), 145–152. http://doi.org/10.1016/j.ijpharm.2011.02.065

Rauk, A. P., Guo, K., Hu, Y., Cahya, S., & Weiss, W. F. (2014). Arrhenius time-scaled least squares: a simple, robust approach to accelerated stability data analysis for bioproducts. *Journal of Pharmaceutical Sciences*, *103*(8), 2278–86. http://doi.org/10.1002/jps.24063

Rinaudo, M. (2006). Chitin and chitosan: Properties and applications. *Progress in Polymer*

719 *Science*, *31*(7), 603–632. http://doi.org/10.1016/j.progpolymsci.2006.06.001

720 Ryan, S. M., McMorrow, J., Umerska, A., Patel, H. B., Kornerup, K. N., Tajber, L., …
721 Brayden, D. J. (2013). An intra-articular salmon calcitonin-based nanocomplex reduces
722 experimental inflammatory arthritis. *Journal of Controlled Release*, *167*(2), 120–129.
723 http://doi.org/10.1016/j.jconrel.2013.01.027

724 Segura-Campos, M., Chel-Guerrero, L., Betancur-Ancona, D., & Hernandez-Escalante, V.
725 M. (2011). Bioavailability of Bioactive Peptides. *Food Reviews International*, *27*(3),
726 213–226. http://doi.org/10.1080/87559129.2011.563395

727 Sharpe, L. A., Daily, A. M., Horava, S. D., & Peppas, N. A. (2014). Therapeutic applications
728 of hydrogels in oral drug delivery. *Expert Opinion on Drug Delivery*, *11*(6), 901–15.
729 http://doi.org/10.1517/17425247.2014.902047

730 Siepmann, J., & Göpferich, A. (2001). Mathematical modeling of bioerodible, polymeric
731 drug delivery systems. *Advanced Drug Delivery Reviews*, *48*(2–3), 229–247.
732 http://doi.org/10.1016/S0169-409X(01)00116-8

733 Silva, N. C., Silva, S., Sarmento, B., & Pintado, M. (2013). Chitosan nanoparticles for
734 daptomycin delivery in ocular treatment of bacterial endophthalmitis. *Drug Delivery*,
735 *7544*, 1–9. http://doi.org/10.3109/10717544.2013.858195

736 Singh, M. R., Singh, D., Saraf, S., & Saraf, S. (2011). Formulation optimization of controlled
737 delivery system for antihypertensive peptide using response surface methodology. *Am J*
738 *Drug Discov Dev*, *1*(3), 174–187. http://doi.org/10.3923/ajdd.2011.174.187

739 Sureshkumar, M. K., Das, D., Mallia, M. B., & Gupta, P. C. (2010). Adsorption of uranium
740 from aqueous solution using chitosan-tripolyphosphate (CTPP) beads. *Journal of*

Hazardous Materials, *184*(1–3), 65–72. http://doi.org/10.1016/j.jhazmat.2010.07.119

Takahashi, M., Uechi, S., Takara, K., Asikin, Y., & Wada, K. (2009). Evaluation of an Oral Carrier System in Rats: Bioavailability and Antioxidant Properties of Liposome-Encapsulated Curcumin. *Journal of Agricultural and Food Chemistry*, *57*(19), 9141–9146. http://doi.org/10.1021/jf9013923

Vimal, S., Abdul Majeed, S., Taju, G., Nambi, K. S. N., Sundar Raj, N., Madan, N., … Sahul Hameed, A. S. (2013). Chitosan tripolyphosphate (CS/TPP) nanoparticles: preparation, characterization and application for gene delivery in shrimp. *Acta Tropica*, *128*(3), 486–93. http://doi.org/10.1016/j.actatropica.2013.07.013

Waterman, K. C., & Adami, R. C. (2005). Accelerated aging: Prediction of chemical stability of pharmaceuticals. *International Journal of Pharmaceutics*, *293*(1–2), 101–125. http://doi.org/10.1016/j.ijpharm.2004.12.013

Weber, C., Coester, C., Kreuter, J., & Langer, K. (2000). Desolvation process and surface characterisation of protein nanoparticles. *International Journal of Pharmaceutics*, *194*(1), 91–102. http://doi.org/10.1016/S0378-5173(99)00370-1

Woranuch, S., & Yoksan, R. (2013). Eugenol-loaded chitosan nanoparticles: I. Thermal stability improvement of eugenol through encapsulation. *Carbohydrate Polymers*, *96*(2), 578–85. http://doi.org/10.1016/j.carbpol.2012.08.117

Yamaguchi, N., Kawaguchi, K., & Yamamoto, N. (2009). Study of the mechanism of antihypertensive peptides VPP and IPP in spontaneously hypertensive rats by DNA microarray analysis. *European Journal of Pharmacology*, *620*(1–3), 71–77. http://doi.org/10.1016/j.ejphar.2009.08.005

763 Yao, M., McClements, D. J., & Xiao, H. (2015). Improving oral bioavailability of
764 nutraceuticals by engineered nanoparticle-based delivery systems. *Current Opinion in*
765 *Food Science, 2*, 14–19. http://doi.org/10.1016/j.cofs.2014.12.005

766 Yoon, H. Y., Son, S., Lee, S. J., You, D. G., Yhee, J. Y., Park, J. H., … Pomper, M. G.
767 (2014). Glycol chitosan nanoparticles as specialized cancer therapeutic vehicles:
768 Sequential delivery of doxorubicin and Bcl-2 siRNA. *Scientific Reports*, *4*, 6878.
769 http://doi.org/10.1038/srep06878

770 Zhou, M., Du, K., Ji, P., & Feng, W. (2012). Molecular mechanism of the interactions
771 between inhibitory tripeptides and angiotensin-converting enzyme. *Biophysical*
772 *Chemistry*, *168–169*, 60–66. http://doi.org/10.1016/j.bpc.2012.05.002

773

Supplementary Material

S1: Fitted results of 3rd order polynomial regression against the PDI, ZP, AE % and particle size for LKP-loaded NPs

Polynomial regression equation: $a + bRatio + cRatio^2 + dRatio^3$	**Coefficient of determination (R^2)**
Size (nm) a= - 284.90 c= - 64.68 b= 293.40 d= 4.51	R^2 = 85.6%
PDI a = 2.31 c = 0.12 b= - 0.88 d = 0.01	R^2 = 83.2%
ZP (mV) a = - 16.80 c = - 6.36 b = 31.05 d = 0.42	R^2 = 76.1%
AE (%) a = 335.60 c = 43.79 b = - 202.40 d = - 2.90	R^2 = 50.2%

S2: Loading capacities of LKP-loaded NPs, n=3

Sample	CL113 (mg/ml)	TPP (mg/ml)	Ratio (CL113/TPP)	LC %
1	1.64	0.21	8.0	2.2±0.01
2	1.52	0.33	4.5	3.3±0.00
3	1.58	0.27	5.9	2.3±0.08
4	1.45	0.40	3.6	2.7±0.03

5	1.39	0.46	3.0	2.8±0.02